INSTITUTE OF PHYSICS PUBLISHING and INTERNATIONAL ATOMIC ENERGY AGENCY NUCLEAR FUSION

Nucl. Fusion **42** (2002) 1184–1192 PII: S0029-5515(02)39915-0

Scaling of the pedestal density in type-I ELMy H-mode discharges and the impact of upper and lower triangularity in JET and ASDEX Upgrade

A. Kallenbach, M.N.A Beurskens[1], A. Korotkov[2], P. Lomas[2], W. Suttrop, M. Charlet[2], D.C. McDonald[2], F. Milani[2], J. Rapp[3], M. Stamp[2], EFDA-JET Workprogramme contributors[a] and ASDEX Upgrade Team

MPI für Plasmaphysik, EURATOM Association, D-85748 Garching, Germany
[1] FOM 'Rijnhuizen', EURATOM Association, Trilateral Euregio Cluster, Nieuwegein, Netherlands
[2] EURATOM/UKAEA Fusion Association, Culham, UK
[3] IPP FZ, EURATOM Association, Trilateral Euregio Cluster, Jülich, Germany

E-mail: arne.kallenbach@ipp.mpg.de

Received 24 December 2001, accepted for publication 3 July 2002
Published 11 September 2002
Online at stacks.iop.org/NF/42/1184

Abstract

Experiments have been performed to disentangle the individual role of upper and lower triangularity on density buildup of lower single null, type-I ELMy H-mode discharges in JET. Comparison with corresponding data from ASDEX Upgrade allowed us to determine a dimensionless representation of the relation between the main chamber recycling and core density and to widen the triangularity variation in the data base. To incorporate the recycling flux density Γ in a dimensionless form, an effective scrape-off layer density $n_{e,SOL} \propto \Gamma^{0.5}$ is introduced allowing us to parametrize and scale the core density by the density rise factor $\bar{n}_e/n_{e,SOL}$. The scaling uses edge-specific definitions of normalized Larmor radius, collisionality and beta. Rewritten in dimensional form, a behaviour is found which is very similar to energy confinement scalings for the ELM-averaged conditions considered here: the density rise factor exhibits an almost linear dependence on plasma current, a weak negative toroidal field dependence as well as power degradation. While a pronounced positive dependence of density buildup on the upper triangularity is observed, no significant correlation with the lower triangularity is found. In particular the dependences on plasma current and upper triangularity emphasize the importance of transport physics for the density buildup.

PACS numbers: 52.25.Fi, 52.25.Ya, 52.55.Fa

1. Introduction

Understanding the physics responsible for the core density buildup is important for the development of successful tokamak reactor scenarios. While high core densities are positively desirable to obtain a high fusion product, high edge densities are connected to positive and negative effects. On the one hand, a high edge density supports radiation from intrinsic impurities and allows the formation of a cold divertor plasma which is necessary for a reasonable target lifetime. On the other hand, rising the edge density by gas puffing degrades H-mode confinement [1]. Therefore, the ratio of core and edge density is an important parameter for performance optimization. An engineering parameter allowing us to vary this ratio is the plasma triangularity δ. For given edge density and energy confinement, increasing the average triangularity leads to an increase of the line-averaged density [2, 3]. This behaviour has been attributed to the improved ballooning stability with rising δ, allowing for higher values of the pedestal pressure [4]. Improved access to second stability with rising triangularity has also been suggested to cause the pedestal pressure increase in JET [5]. However, ballooning mode theory does not explain how the increased pressure is distributed between temperature

[a] See annex of Pamela J. *et al* 2001 Overview of recent JET results and future perspectives *Proc. 18th Int. Conf. on Fusion Energy 2000 (Sorrento, 2000)* (Vienna: IAEA).

and density, and the scaling of the pedestal width is also not clear [6].

An interesting question is whether the divertor or main chamber physics are more important for the core density buildup. In ASDEX Upgrade (AUG), the core density was found to be closely linked to main chamber recycling [1], while the separatrix density changed with the divertor design. Changing from AUG Divertor I to Divertor II, the typical ELM-averaged separatrix density increased from about 0.4 to 0.6 of the line-averaged density with moderate fuelling [7]. The ratio of pedestal and separatrix density was found to vary only weakly under ELMy H-mode conditions and was mainly determined by the proximity to the Greenwald limit in Divertor II [8]. Changing from Divertor I to Divertor II did not significantly effect the main chamber recycling for given core parameters. Closing the divertor just increased the neutral flux in the divertor. In contrast, reducing the bypass leaks in the JET Mark IIA divertor by 75% and becoming Mark IIAP reduced the main chamber neutral pressure by about 35%, demonstrating that escaping divertor neutrals can be important in the main chamber for an open divertor geometry [3].

In JET, no routine and direct measurements of the separatrix density were available for H-mode conditions in the past. Available lithium beam measurements of the edge density profiles showed very low relative separatrix densities $n_{e,sep}/\bar{n}_e \approx 0.15$ for unfueled H-mode conditions [9], with a trend to higher ratios during gas puffing. Onion-skin modelling, based on target profiles from Langmuir probe measurements, revealed a broad range of separatrix and core densities, with the tendency towards rising separatrix to core density ratio with gas puffing [10].

Inside the H-mode pedestal top, particle transport is usually modelled with moderate values of the inward pinch v_{in} of the order $1\,m\,s^{-1}$ [11]. However, the steep edge gradients outside the pedestal are often not treated in detail. Since particle fluxes are present in this region, an effective diffusion coefficient is sufficient to model the density profile shape. Modulated particle transport techniques capable of measuring D and v individually are usually not applicable in the edge transport barrier region. Therefore, little is known about the particle transport coefficients in this region.

In this paper, the idea is pursued that variations of plasma transport have a large impact on pedestal and core density buildup, which can be described by dimensionless quantities provided an appropriate set of variables is found. Only type-I ELMy H-mode conditions are considered here, where the proximity to a stability threshold seems to be important for the transport behaviour. For example in the L-mode, the beneficial effect of triangularity on density buildup is much weaker or not present, suggesting that different physics is important under these conditions. The parametrization of the density profiles is made using the dimensionless expressions ρ^*, ν^* and β_t [12, 13] used in a special definition suitable for the plasma edge. This corresponds to a collisonal high-β ansatz for the underlying transport [14]. Particular emphasis is put on the plasma triangularity δ which is known to have big impact on high density H-mode performance.

The paper is organized as follows. In section 2 JET experiments on triangularity variations are introduced which deliver the experimental input on the individual variation of upper and lower triangularity. A dimensionless ansatz for the pedestal density is developed in section 3, using an effective edge density derived from main chamber recycling. Scaling relations for a broad range of experimental parameters are derived employing data from the JET (Mark IIGB divertor) and AUG (Div II divertor) tokamaks. In section 4 possible physical mechanisms behind the obtained scaling relations are discussed.

2. Global influence of upper and lower triangularity

The beneficial effect of plasma triangularity on high density H-mode operation was first studied during gas scan experiments in JET [2]. An equal effect of upper and lower triangularity was assumed in the interpretation of the experiments, employing the mean triangularity $\delta_{mean} = (\delta_{up} + \delta_{low})/2$ as ordering parameter. Since the upper triangularity was predominantly varied in these experiments, δ_{mean} and δ_{up} are equal ordering parameters. Investigations of the triangularity dependence of the pedestal pressure in AUG could also not resolve the individual roles of upper and lower triangularity due to operational constraints [15].

Therefore, dedicated plasma shape variations have been performed at JET to disentangle the individual roles of upper and lower triangularity. Figure 1 compares discharges with different δ_{up} and δ_{low} with 2.5 MA plasma current, more than 12 MW neutral beam injection and no external gas fuelling. With rising triangularity, line-averaged density and Greenwald factor increase considerably while the energy confinement rises slightly. However, since the shape variation also alters the divertor configuration and the recycling flux pattern, a broader experimental data base is required to verify the different effect of δ_{up} and δ_{low}.

In the following, we perform a regression analysis of steady state time slices like those shown in figure 1 representing ELM-averaged data averaged over at least two energy confinement times. As an example and to illustrate the influence of triangularity variation, figure 2 shows a simple analysis based on global quality factors for a subset of the JET data with plasma currents I_p around 2.5 MA, about 13 MW NBI heating power and various gas fuelling levels. The triangularity dependence is evaluated for the performance parameter $f_{Green} \times H_{89p}$, which showed a high sensitivity on triangularity variations. The line-averaged density, f_{Green} is normalized to the Greenwald density and H_{89p} the energy confinement time normalized to the ITER-89p L-mode prediction [16]. A clear correlation of the performance parameter with the upper triangularity is seen, while δ_{low} shows no significant correlation. Raising δ_{up} leads in particular to a higher density for a given fuelling rate, which is beneficial since fuelling normally degrades the H-mode confinement [2, 1]. The best high triangularity points in figure 2(b) are obtained with moderate fuelling, achieving $f_{Green} = 1$ and $H_{89p} = 2$ simultaneously. However, the quantification of an unsymmetric effect of δ_{up} and δ_{low} is hampered by the lower variation range of δ_{low}. A dedicated scan of the lower triangularity at high δ_{up} is included in the data points at the top of figure 2(a). The discharges with reduced δ_{low} in this scan show a somewhat reduced performance parameter and changed ELM behaviour, in accordance with the hypothesis that the

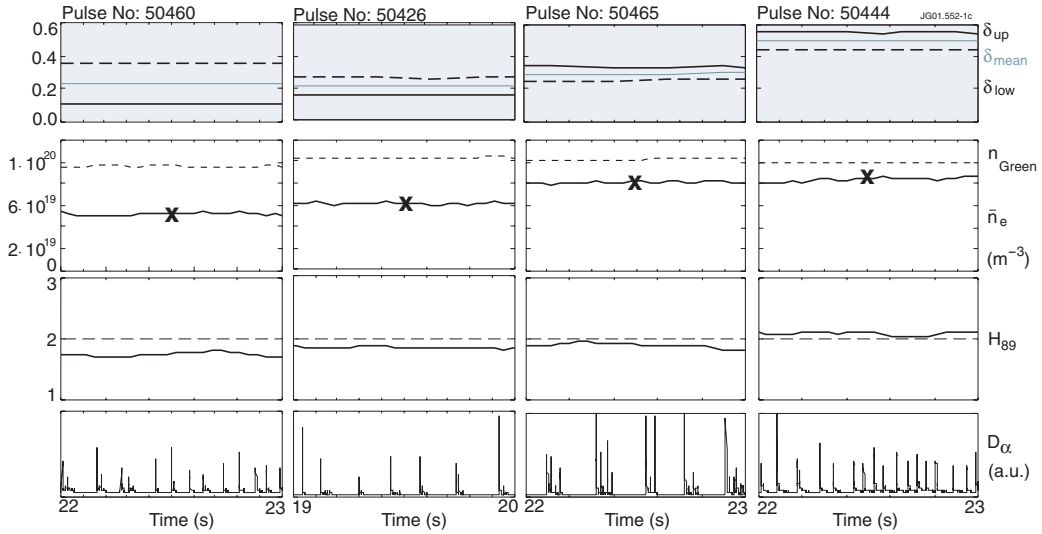

Figure 1. Comparison of discharges with different upper (——) and lower (- - - -) triangularities in JET. Shown here are the line-averaged density from interferometry, the Greenwald density and the confinement normalized to the ITER-89p scaling as well as divertor D_α traces marking the ELM behaviour. The black crosses mark the prediction of the scaling equation (7). $I_p = 2.5$ MA, $B_t = 2.4$ T, $P_{heat} \approx 13$ MW, no external gas fuelling.

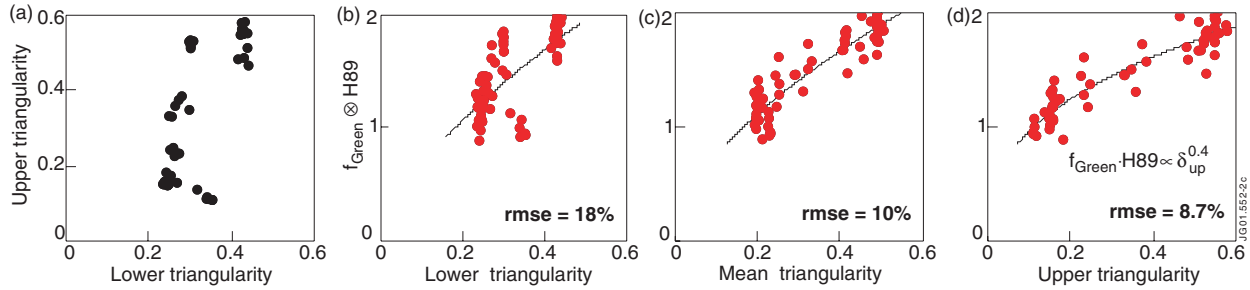

Figure 2. Subset of data with similar plasma current (2.4–2.9 MA), $P_{heat} > 12.5$ MW and gas fuelling between 0 and $4 \cdot 10^{22}$ at. s^{-1} demonstrating the different influence of upper and lower triangularity. (*a*) δ_{up}, δ_{low} parameter space covered including dedicated triangularity variation experiments. (*b*)–(*d*) show the performance parameter $f_{Green} \times H_{89p}$ versus lower, mean and upper triangularity, respectively. δ_{up} gives the best fit of the performance.

mean triangularity is the most appropriate parameter for energy confinement. An analysis of the effect of triangularity on thermal confinement is given in [17]. The reduction of the energy confinement with decreasing δ_{low} is accompanied by an increased ELM frequency. On the other hand, the relation of line-averaged density and recycling, a measure for particle confinement, is not reduced with lower δ_{low}, indicating a different behaviour of particle and energy transport.

A major problem for the disentanglement of the individual effects of upper and lower triangularity on density buildup is the change of divertor configuration and recycling pattern with δ_{low}. Correlations of these changes with the experimental observations, e.g. on performance make it difficult to identify the underlying causality. To gain additional information, data from the AUG tokamak are taken into account which exhibit a quite different triangularity and divertor configuration range, while aspect ratio and elongation are very similar to JET. Since the density behaviour plays a key role in triangularity variations, and corresponding input data are coherently available in both machines, the following analysis concentrates on the line-averaged core density measured by interferometry and the hydrogen flux density in the midplane derived from H_α spectroscopy.

3. Dimensionless density scaling

3.1. Density profile parametrization

A typical density profile in JET is shown in figure 3. Two timepoints of the LIDAR systems are plotted to point out the data quality. Lithium beam [5] and edge LIDAR diagnostics [18] overlay well in this case.

The density profile inside the separatrix is very steep, while the core electron density profiles are usually flat under H-mode conditions. A sharp transition is expected between the steep gradient and flat core zone, forming a density shoulder. The top of the steep region is the pedestal. Under H-mode conditions the gradients obtained from the edge LIDAR system are limited by the spatial resolution of the diagnostic, and the density pedestal width cannot be determined [19].

A general problem of edge profile analysis is the necessary mapping by means of the magnetic equilibrium [20]. Due to the steep edge profiles, uncertainties in the separatrix position of up to 2 cm turn into considerable uncertainties of n_e for a given flux surface label. This is in particular a problem for the Lithium beam diagnostic, which has a slightly better spatial resolution compared to the edge LIDAR system.

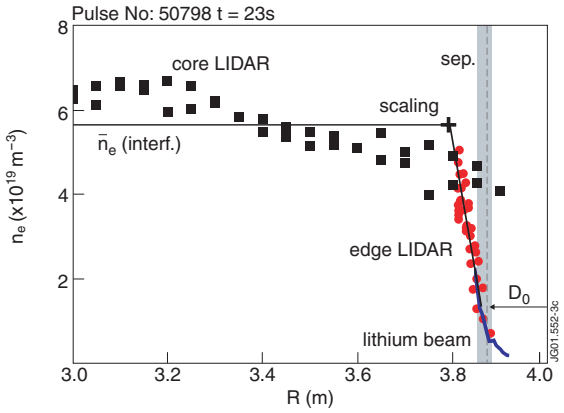

Figure 3. Density profile for a stationary, medium gas-puff, type-I ELMy H-mode discharge with medium-high triangularity in JET ($I_p = 2$ MA, $f_{Green} = 0.75$, $\delta_{up} = 0.38$). Data points correspond to 2 time points of the core and edge LIDAR systems. The grey line shows the edge density from the lithium beam diagnostic of a very similar pulse (50799). The 3 outer points of the core LIDAR system are not reliable due to the low spatial resolution of this system and possible misalignement [18]. The vertical grey band indicates the range of possible separatrix positions according to EFIT mapping, the horizontal arrow refers to $n_{e,SOL}$ derived from equation (1).

Unfortunately, both Li-beam and LIDAR system do not reach the pedestal top for usual conditions, and different diagnostics have to be connected to construct the full profile causing mapping to become a problem.

To overcome the mapping and resolution problems, the density profile is parametrized here in a very simple way: the pedestal density is approximated by the line-averaged value obtained by interferometry, while an effective edge density is derived via the D_α recycling flux. It should be noted that the pedestal density is expected to be about 0.8× the value of the line-averaged density for typical conditions, but the directly measured $\bar{n}_e$ is used throughout this paper. Within this simple model, the density pedestal width is $w = (0.8 \times \bar{n}_e - n_{e,SOL})/\nabla n_e$. Direct measurements of w in JET are not available for H-mode conditions so far. Estimations based on the JET Lithium beam diagnostics suggest H-mode values for w around 2–4 cm in the outer midplane. In AUG edge Thomson scattering in combination with radial sweeps [21] available for a subset of discharges yields values for w around 1.5 cm.

Core density peaking is not considered in this paper, scenarios with pronounced density profile peaking have therefore been ruled out. A study on central fuel ion transport in JET, omitting the edge transport barrier region, is given in [22].

3.2. Choosing the dimensionless quantities

In the following, we search for a dimensionless scaling expression for the pedestal electron density, which is equated with the line-averaged density for simplicity and due to the lack of good profile data around the density shoulder. Scaling with dimensionless parameters has the advantage that constraints given by the parameter definitions automatically give the correct size scaling (wind tunnel approach), provided that the parameters chosen represent the valid physics. We have chosen the normalized gyro-radius ρ^*, the normalized collisionality ν^* and the normalized pressure β_t in an edge specific definition motivated by the availability of robust input data. There is no beforehand justification for this ansatz, in particular for the edge, where atomic physics in terms of temperature may be important. Lackner discussed the inclusion of a normalized temperature for similarity studies regarding divertor performance [23]. The identity requirement for at least one of the four parameters has to be dropped then to define a non-trivial set of equivalent devices. A candiate to drop in edge physics would be β_t. However, transport in the edge barrier region is expected to depend on β, e.g. via the effect of the edge bootstrap current on stability. The criterium to decide about the most appropriate set of dimensionless parameters used here is which parameter set gives the best fit of the experimental data in both JET and AUG.

Since the value of the core density is determined in the region between the wall and a few cm inside the separatrix, the relevant dimensionless parameters have to be evaluated at the plasma edge. Well resolved and accurate density and temperature profiles are generally not available in this region, therefore characteristic values have to be used, which can be directly measured or indirectly derived routinely.

The characteristic temperature chosen is the upstream separatrix electron temperature, T_u, as obtained from a simple 2-point divertor model based on parallel electron thermal conductivity. The choice of the characteristic density was led by the requirement to use an 'engineering' quantity to obtain an expression for the absolute density value. If a part of the density profile was used as a parameter for an expression for $n_{e,ped}$, then only the relative shape could be described. We chose the recycling flux measured by midplane D_α spectroscopy. The D_α photon flux is almost proportional to the ionizing influx of neutrals in the plasma edge, and has been successfully used to model fuel particle transport using trace tritium measurements in JET [22]. This flux may have contributions due to ion outward diffusion, divertor escaping neutrals and plasma-wall interaction due to ELMs. In practice, the recycling level has a lower limit connected to wall load and conditioning, while its maximum value is related to the H-mode density limit. In between these limits, the recycling is externally controlled by the gas feed and can be considered an engineering parameter.

To be suitable for the scaling purposes, the D_α photon flux Γ_{D_α}, which represents the recycling flux, has to be converted into a density. This is done by a simple high recycling ansatz for the SOL density, which has been normalized to electron density measurements with a lithium beam diagnostics in the SOL of AUG [1].

$$n_{e,SOL} = 2.7 \cdot 10^9 \,\mathrm{m^{-2}\,s^{1/2}} (\Gamma_{D_\alpha}\,(\mathrm{m^{-2}\,s^{-1}}))^{1/2} \qquad (1)$$

Γ_{D_α} is measured along a horizontal/radial viewing line emerging near the outer midplane. The density value obtained is a representative value connected to the source in the edge plasma, corresponding roughly to the lower end of the steep gradient zone (see figures 3 and 8). The dimensionless edge parameters are defined as follows:

$$\rho^* = 1.445 \cdot 10^{-4} \frac{(m_i \cdot T_u)^{0.5}}{R_{geo} \cdot B_t}$$

$$\nu^* = 1 \cdot 10^{-16} \frac{n_{e,SOL} \cdot R_{geo} \cdot q_{95}}{T_u^2}$$

$$\beta_t = 8 \cdot 10^{-25} \frac{n_{e,SOL} \cdot T_u}{B_t^2} \qquad (2)$$

where m_i is the ionic mass number. The upstream temperature T_u is taken in eV and calculated from the parallel electron conductivity assuming $T_{target} = 0$ as the boundary condition.

$$T_u = \left(\frac{3.5 P_{net} \cdot l_{con}}{A_{SOL\|} \cdot \kappa_0} \right)^{2/7} \tag{3}$$

The power flowing in the SOL, $P_{net} = P_{heat} - P_{rad}$ is approximated using the total heating power and the global radiation measurements as routinely available in JET and AUG. Taking radiation profiles into account would overstress the simple ansatz of equation (3). A simple estimate for the connection length is used, $l_{con} = \pi q_{95} R_{geo}$ [24]. We use $\kappa_0 = 2000\,(\mathrm{W/m})\,\mathrm{eV}^{-7/2}$ omitting the Z_{eff} dependence so far since the edge Z_{eff} is not well known. The effective SOL cross section for heat flow

$$A_{SOL\|} = 4\pi R_{geo} \lambda_{q\|} \frac{B_p}{B}, \qquad \lambda_{q\|} = \frac{2}{7} \lambda_T \tag{4}$$

depends on the midplane power decay length $\lambda_{q\|}$, which is assumed to be $\frac{2}{7}$ of the temperature decay length λ_T. It is convenient to use an ansatz for λ_T that leads to cancelling of the magnetic field line angle term B_p/B:

$$\lambda_T = 2.5 \cdot 10^{-3} \frac{B}{B_p} \ \mathrm{(m)} \tag{5}$$

Equations (1)–(5) represent a simplified ansatz for the construction of dimensionless parameters, constrained by the accessibility of the input parameters. In particular, the representative values of edge temperature and density are not strictly taken at the same position, as no clear radial location can be assigned to the effective $n_{e,SOL}$ derived from the recycling flux. Therefore, one implicit assumption made in the parameter choice is the radial coupling or correlation of edge transport, as it would be supplied by the presence of intermittent convection [25, 26].

3.3. Scaling results

A regression analysis was done for time-averaged data of about 150 time slices in steady state H-mode discharges in JET and AUG. In order to stick to dimensionless units, the normalized density $\bar{n}_e/n_{e,SOL}$ was scaled versus the quantities ρ^*, ν^* and β_t according to equation (2) as well as the safety factor, q_{95}, and the upper and lower triangularity δ_{up} and δ_{low}. Elongation and aspect ratio were not used as variables due to their small variation in the data set. The mean values are $\bar{\kappa} = 1.72$ and $\bar{\epsilon} = 0.30$ and are very similar for JET and AUG. In order to keep the impact of Z_{eff} variations limited for this study, the data set has been restricted to time slices with $\bar{Z}_{eff} < 2.5$, because no reliable measurements of Z_{eff} at the edge were available. Simulations of neon-seeded discharges in AUG with the 1.5-D BALDUR transport code suggests an influence $\nu_{in}/D \propto Z_{eff}$ [27]. The result of the regression analysis gives a good description of the normalized densities in JET and AUG:

$$\frac{\bar{n}_e}{n_{e,SOL}} = 32.7 \nu^{*0.285} \rho^{*0.892} \beta_t^{-0.796} q_{95}^{-0.97} (\delta_{up} + 0.2)^{0.372} \tag{6}$$

Error analysis of the regression fit supplies the following standard deviations of the exponents: $\nu^* \pm 0.1$, $\rho^* \pm 0.13$, $\beta_t \pm 0.1$, $q_{95} \pm 0.18$, $(\delta_{up} + 0.2) \pm 0.06$.

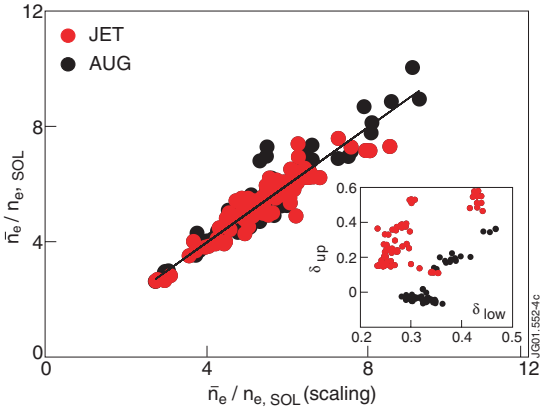

Figure 4. Normalized density versus the prediction of the dimensionless scaling. The inset shows the triangularity space covered by the data from both machines.

The dependence on the lower triangularity is $\bar{n}_e/n_{e,SOL} \propto (\delta_{low} + 0.2)^{0.00\pm0.22}$ or $\propto \delta_{low}^{0.00\pm0.14}$. Therefore, the asymmetry of the density with respect to upper and lower triangularity appears to be statistically significant. Figure 4 shows the normalized experimental density versus the prediction of the scaling for both JET and AUG. The triangularity range covered by the AUG discharges has on average a higher δ_{low} and a lower δ_{up} in comparison to JET.

It is worthwhile to inspect also the dimensional form of the scaling equation (6). By inserting the definitions of ρ^*, ν^* and β, we obtain

$$\bar{n}_e = 3.3 \cdot 10^{17} \Gamma_{D_\alpha}^{0.2445} P_{net}^{-0.263} q_{95}^{-0.944} B_t^{0.7} \times R_{geo}^{-0.607} (\delta_{up} + 0.2)^{0.372} \tag{7}$$

This is, within the assumptions made, the dimensional correct expression using the engineering parameters allowing an easier comparison with other tokamaks. The exponent for the D_α flux density must be taken with the given accuracy since the numerical value is large in SI units. Notable is the weak dependence of $\bar{n}_e$ on the recycling flux. This reflects the well-known resilience of the H-mode density.

A direct regression with these dimensional quantities yields

$$\bar{n}_e \propto \Gamma_{D_\alpha}^{0.257} P_{net}^{-0.25} q_{95}^{-1.02} B_t^{0.71} R_{geo}^{-0.71} (\delta_{up} + 0.2)^{0.398} \tag{8}$$

The standard deviations of the fit exponents are as following: $\Gamma \pm 0.04$, $P_{net} \pm 0.07$, $q_{95} \pm 0.2$, $B_t \pm 0.13$, $R_{geo} \pm 0.18$, $(\delta_{up} + 0.2) \pm 0.07$. Since the constraints by the dimensionless ansatz were given up, the number of free parameters in the fit increased by one. The fact that equations (7) and (8) are quite similar and that the root mean square error was not reduced with the additional fit parameter is a hint that the relevant physics is covered by the ansatz equation (6). As a further test, we also exchanged each of the dimensionless parameters in equation (2) by the temperature T_u, as suggested for the case that atomic physics is important [23]. The resulting fits showed a significantly degraded quality in comparison to equation (6).

The expression equation (7) allows for a good prediction of the line-averaged electron density for type-I ELMy H-modes in the JET and AUG tokamaks, as shown in figure 5. The scaling obtained allows to visualize the impact of the triangularity for

a wide range of experimental conditions. Figure 6(*a*) shows the measured density normalized by the prediction reduced by the triangularity factor. The dependence on δ_{up} can be clearly seen, the ansatz with $\delta + 0.2$ in the scaling gives a good description over the range of δ_{up}. A pure exponential ansatz for the triangularity effect is not possible since negative values of δ_{up} occur in AUG (see inset in figure 4). Even for small positive values for δ_{up}, large relative variations of δ^x occur. Without the physics behind the triangularity effect known, the +0.2 ansatz was found by minimizing the root mean square error of the measured density with respect to the scaling prediction. Adding the value 0.2 gives a better fit than adding 0.1 or 0.3. The added constant value determines the relative weight of the triangularity variation on the density for high and low values of δ_{up}.

If there would be a significant dependence on δ_{low}, this should show up in figure 6(*b*), where the ratio of measured and predicted density is plotted versus the lower triangularity. The lacking effect of δ_{low} is seen in all versions of the density scaling so far, dimensional and dimensionless, obtaining exponents for the δ_{low} dependence between 0 and −0.1 with a typical uncertainty of ±0.15.

Since the asymmetry of the upper and lower triangularity effects is not expected from simple stability considerations, another visualization of the effect is shown in figure 7. Here, the deviation of the density from the scaling prediction (scaling without the δ_{up} dependence and normalized to 1 for the average data) is colour coded in the (δ_{up}, δ_{low}) plane. Although the experimental variation of the lower triangularity has a much smaller range than δ_{up}, the δ_{low} range being predominantly limited by divertor configuration constraints, the lacking of the density variation with δ_{low} can be clearly seen.

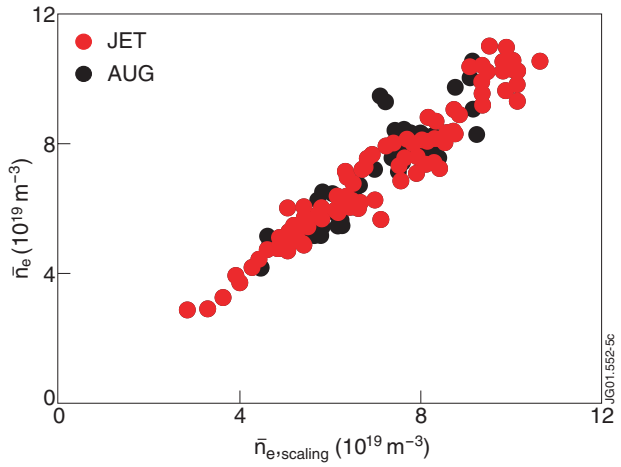

Figure 5. Measured versus predicted absolute density for various experimental conditions in JET and AUG H-mode discharges.

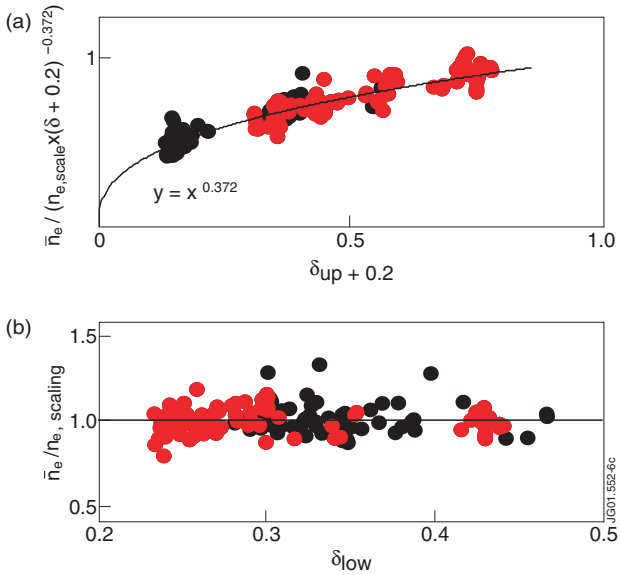

Figure 6. (*a*) Measured density, normalized by the reduced scaling law with omitted triangularity factor, versus upper triangularity. (*b*) Ratio of measured density and scaling prediction versus lower triangularity.

3.4. *Interpretation*

What is the physical meaning of the parameter $\bar{n}_e/n_{e,SOL}$? Previous work on the density profile behaviour in AUG suggests the presence of an anomalous particle inward pinch around the separatrix [28]. The introduction of a pinch is related to the fact that the thick scrape-off layer does not allow a sufficient amount of neutrals to penetrate deep enough to provide a sufficient particle source up to the pedestal top. In the most simple ansatz for the particle transport, setting the line-averaged density equal to the pedestal density and neglecting the neutral sources inside the location of $n_{e,SOL}$, the density rise factor is

$$\frac{\bar{n}_e}{n_{e,SOL}} = \exp\left(\frac{w \cdot v_{in}}{D}\right) \tag{9}$$

with the gradient region width w, diffusion coefficient D and inward pinch velocity v. D and v closely inside the separatrix of AUG have been determined for silicon from the profile evolution in between ELMs [29]. Typical values are $D = 0.5\,m^2\,s^{-1}$ or below and $v_{in} = 20\,m\,s^{-1}$ for silicon in a low triangularity discharge. The inward drift velocity v_{in} of impurities is expected to be at least partly caused by neoclassical effects, as shown in ALCATOR C-Mod [30]. Consequently, lower values for the transport parameters of the fuel ions are expected. Values for the transport barrier diffusion coefficient D of $0.01\,m^2\,s^{-1}$ in ELM-free H-modes and $0.1\,m^2\,s^{-1}$ in type-III ELMy H-modes are reported in [30]. Integrated core-edge simulations of ELMy H-modes in JET with the COCONUT code used an inward pinch of $5\,m\,s^{-1}$ for both impurity and fuel ions in the boundary region up to the pedestal top, but no sensitivity study on the significance of this value is given [31]. To explain the typical density rise factor obtained, a possible combination of coefficients according to equation (9) could be $D = 0.2\,m^2\,s^{-1}$, $v = 10\,m^2\,s^{-1}$ and $w = 0.03$ m, resulting in $\bar{n}_e/n_{e,SOL} \approx 4.5$.

For a given pedestal density, the assumed fuel ion inward pinch has to be reduced with increasing neutral sources and with decreasing value of the diffusivity D. Mahdavi *et al* [32, 33] describe the density pedestal width in DIII-D by a simple analytical model for neutral penetration, taking charge the exchange acceleration of the neutrals into account. Introducing a geometry factor $f(\theta_0) \approx 2.5$ to account for the larger flux expansion in the X-point region, they are able to explain the density pedestal width by the neutral penetration,

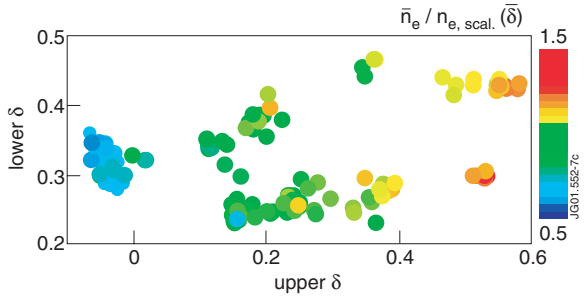

Figure 7. Colour coded deviation of the measured electron density from the scaling prediction with the δ_{up} dependence omitted. For normalization, the scaling equation (7) has been evaluated with the averaged triangularity in the data base, $\bar{\delta}_{up} = 0.21$.

which they find to be quite independent of the diffusivity in the barrier region.

Only midplane measurements of the recycling level are used in this study, therefore we do not differentiate between the main chamber and divertor recycling, and direct fuelling by divertor neutrals is not taken into account. If the ratio of neutral densities in the midplane and in the vicinity of the X-point is varied, e.g. by strong puffing and pumping, the poloidal source distribution and consequently the pedestal density can be effected. In this study, no strong puff and pump technique is applied, and the total main chamber recycling level dominates over the gas input and the pumped particle flux. Therefore, variations of the neutral source caused by changes of the poloidal neutral distribution, which would correspond to a variation of the factor $f(\theta_0)$ in [32], are expected to be small here. Since the density gradient region in the edge is not resolved under H-mode conditions in JET so far, a comparison with the pedestal width model [32] is not yet possible, and the relative importance of the neutral source versus a hypothetical inward pinch or gradient/stability criterion is not resolved. The presence of ELMs in addition complicates the comparison with simple models.

To display the experimental situation for direct edge density profile comparisons, the most similar shots in dimensionless parameters according to equation (2) in the combined JET–AUG database are compared in figure 8. Dimensionless similarity requires a high plasma current in AUG and a low current in JET compared to typical values of the devices, respectively. The edge density profiles are measured by Lithium beam diagnostics. The AUG discharge has relatively high density, and consequently the lithium beam has a short penetration depth.

The discharges compared in figure 8 are quite similar in the edge related dimensionless parameters as well as (within 15%) with respect to core-related parameters ρ^*, ν^*, and β_t obtained from $\bar{n}_e$ and total stored energy. The profiles in both machines seem to be shifted versus each other in radial direction, but the deviation is still compatible with the radial mapping accuracy. A recent re-analysis of AUG Li-beam data and comparison to edge Thomson measurements suggest a radial inward shift of 1 cm [34], bringing the normalized AUG and JET profiles close to each other.

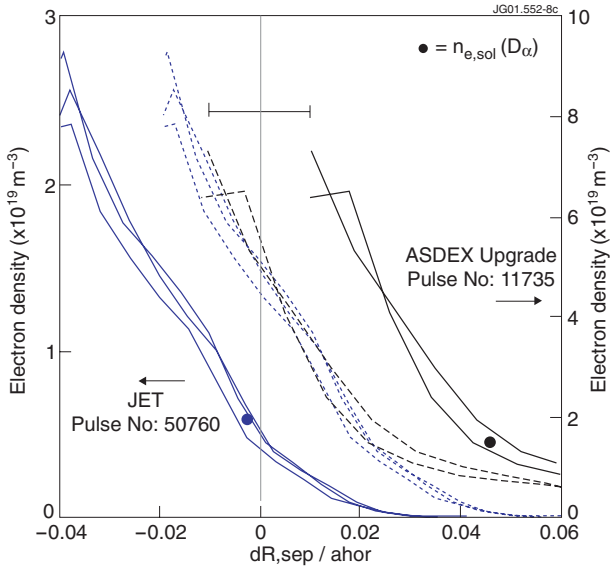

Figure 8. Edge density profiles from Lithium beam measurements for dimensionless similar discharges in JET and AUG versus distance from separatrix normalized by the minor radius. The AUG data were evaluated in between ELMs to avoid perturbation of the Li beam analysis, the dashed profiles are shifted 1 cm towards the inside in accordance with a recent data reanalysis. The JET lithium beam data are also shown shifted outward by the radial position uncertainty (dashed profiles). The profiles from both machine agree within the radial error bar inside the outer SOL and exhibit the same slope when scaled according to the dimensionless ansatz: the density in AUG is expected to be larger by the squared inverse ratio of the major radii, factor 3.2. The innermost wall contact of the JET equilibrium is at dR, sep /ahor ≈ 0.035, the corresponding AUG value is 0.07. The line-averaged densities are 3.2 for the JET pulse and $9.1 \cdot 10^{19}$ m^{-3} for AUG, respectively.

4. Discussion

The physical picture of core density buildup developed here is based on an effective scrape-off layer density, described in terms of the recycling flux, which is coupled to the wall by radial ion fluxes and subsequent wall recycling, as recently reported from Alcator C-Mod [35]. Due to its low time resolution, the H_α diagnostics used here delivers only time- and space-averaged fluxes with respect to the scales of edge plasma filaments. Possibly, a fraction of the particles is carried by fast plasma blobs moving radially outward by $E \times B$ drifts caused by ∇B plasma polarization [36, 26]. These blobs may produce density shoulders in the time averaged edge density profiles, as often observed in AUG with gas puffing [37]. The neutral fluxes caused by radial ion fluxes are supplemented by neutrals escaping out of the divertor contributing to the main chamber neutral flux. Estimates based on the bypass conductances give values significantly lower than the measured neutral flux densities. The different contributions are hard to distinguish, because the main chamber and divertor recycling scale very similar with $n_{e,sep}$.

The H-mode transport barrier extends between the locations of the SOL density and the core density pedestal top (see figure 8). The density gain factor over the barrier region is given by equation (6) or equivalently (7). It is not clear what is the governing physics leading to the observed behaviour. If the diffusivity in the ETB region is very small,

(below $0.1\,\mathrm{m^2\,s^{-1}}$), the neutral sources can explain the pedestal density. For larger values of D, an inward pinch is required. In addition, stability criteria related to microturbulence may play a role, as suggested by the parameter dependence of equation (7), in particular the dependences on plasma current, shaping and heating power.

No theoretical models for an edge particle inward pinch are available up to now, neoclassical effects like the Ware pinch are by far too small to be compatible with the observations. Ion temperature gradient driven modes (ITG) and electron temperature gradient driven modes (ETG) have been found responsible for heat transport over a broad temperature range. However, particle transport has not been paid much attention for so far in theoretical ITG and ETG mode investigations. Radial correlation lengths of density fluctuations have recently been measured in AUG with a swept single-frequency reflectometry system [38]. For H-mode conditions, the correlation length is found to rise with β, suggesting the importance of electromagnetic effects like Alfvén drift waves [39] although the absolute values of β are low in the edge region.

The observed dependence of $\bar{n}_\mathrm{e}/n_\mathrm{e,SOL}$ on shaping and plasma current hints towards the importance of stability criteria, or more precisely the parameter dependence of the stability-limited edge pressure gradient. The generally supposed origin of the beneficial effect of the triangularity on performance is an increased ballooning stability, which allows for the development of a higher pedestal pressure (a review of experimental observations and theoretical modelling of pedestal and edge transport barrier is found in [6]).

The relevant parameter for ballooning stability is the edge local magnetic shear in the region of bad curvature, which in general trend rises with triangularity. Calculations of the edge magnetic shear requires the inclusion of edge currents and pressure gradient measurements, which are not routinely available with sufficient precision. In addition, stability theory does not predict how the pressure gradient is distributed into temperature and density gradients. The bootstrap current itself has a different dependence on temperature and density gradients, leading to a complex situation calling for a self-consistent treatment of transport and stability in the edge transport barrier region, which is not available so far. First evidence for the coupling of density and temperature gradients in the ETB region has been obtained recently in AUG by edge Thomson scattering. The normalized gradient ratio $\eta_\mathrm{e} = \mathrm{d}\log(T_\mathrm{e})/\mathrm{d}\log(n_\mathrm{e})$ has been found to be constant and about 2 from the pedestal top into the hot part of the scrape-off layer [37].

A quite surprising observation is the asymmetry of the pedestal density with respect to upper and lower triangularity for given neutral flux. A possible explanation could be given by a stabilizing effect of the X-point magnetic topology due to the variation of the local shear in the vicinity of the X-point [40]. Such a stabilizing effect of the X-point could anticipate the stabilizing effect of an increased lower triangularity in these lower single null plasmas. Another asymmetry in particle transport with respect to upper and lower triangularity is the presence of higher neutral fluxes around the lower X-point in the lower single-null configurations investigated here.

In contrast to the particle transport, energy transport shows a more symmetric dependence on upper and lower triangularity. The comparison of similar discharges with large δ_up and varying δ_low showed a reduced energy confinement in combination with an increased ELM frequency for lower δ_low [17], as expected for the mean triangularity being the relevant parameter for energy transport. In contrast, the density behaviour in these discharges corresponds to the scaling equation (6) and exhibits no dependence on δ_low. This different behaviour could be caused by a lesser impact of ELMs on density compared to stored energy.

Not much work is available in the literature about systematic alternating variations of upper and lower triangularity. In Alcator C-Mod, the accessibility of ELM-free and EDA H-modes has been investiated by separate scans of δ_up and δ_low. No evidence for an asymmetric impact of δ on the ELM-free/EDA boundary is reported [41].

Self-consistent stability and (particle) transport calculations are required to explain the observed behaviour, combined with improved edge measurements. Although work has already started [42], the limited resolution of experimental data and the lacking knowledge about energy and particle transport in the edge region will prevent a fast solution of the open questions.

5. Conclusions

This study on H-mode edge densities was motivated by the experimental observation that H-mode performance, e.g. measured in terms of the product of H-factor and Greenwald factor, rises with plasma triangularity. The increased performance is seen in the development of a higher density for a given recycling level, maintaining good confinement at high density. As a consequence, the development of the plasma density plays a key role for the improved performance at elevated triangularity.

We developed an empirical scaling law for the core electron density in type-I ELMy H-mode discharges in JET and AUG. The scaling is based on a special ansatz using dimensionless parameters ρ^*, ν^* and β_t suitable for edge physics. Its success to predict the line-averaged electron density in JET and AUG over a broad range of experimental parameters and the dependence on shaping and plasma current suggest that transport physics or stability play an important role in the core density buildup.

The derived scaling allows to normalize the electron density for various experimental parameter variations, and therefore to disentangle the effects of upper and lower triangularity by comparing quite different discharges. As a result, good evidence is found that the upper triangularity plays the dominant role for the core density buildup in lower single-null H-mode discharges in JET and AUG.

Although the asymmetrical impact of δ_up and δ_low is founded on observations in two tokamaks, it cannot be fully ruled out that the change of divertor configuration and recycling pattern supplies the underlying mechanism. This suggests also an investigation of the ELM behaviour and ELM-induced transport for variations of δ_up and δ_low. So far, only ELM-averaged conditions were considered, and the resulting scalings represent the combined effects of ELM-induced and inter-ELM transport.

For a proper theoretical treatment of the problem, a self-consistent treatment of transport and stability in the edge barrier will be required, which is not available so far. It is hoped that this study can motivate further work, in particular on possible mechanisms for asymmetries of particle transport with respect to triangularity.

Acknowledgments

This work has been performed under the European Fusion Development Agreement. It is a pleasure to acknowledge the commitment of all the people involved in operation, diagnostic and data evaluation at JET. We are indebted to Jim Strachan for acting as Session Leader and for useful comments, to G.F. Matthews for interesting discussions and to Hans-Werner Müller for careful evaluation of AUG lithium beam data.

References

[1] Kallenbach A. *et al* 1999 *Plasma Phys. Control. Fusion* **41** B177
[2] Saibene G. *et al* 1999 *Nucl. Fusion* **39** 1133
[3] Horton L.D. *et al* 1999 *Nucl. Fusion* **39** 1
[4] Osborne T.H. *et al* 2000 *Plasma Phys. Control. Fusion* **42** A175
[5] Korotkov A.A. *et al* 2000 Edge plasma pressure profile evolution in type I ELM discharges on JET *27th Conf. on Controlled Fusion and Plasma Physics (Budapest, Hungary, 2000)*
[6] Hubbard A. 2000 *Plasma Phys. Control. Fusion* **42** A15
[7] Schweinzer J. *et al* 1999 *J. Nucl. Mater.* **266–269** 934
[8] Borrass K. *et al* 1999 *Nucl. Fusion* **39** 843
[9] Breger P. *et al* 1998 *Plasma Phys. Control. Fusion* **40** 347
[10] Erents S.K. *et al* 2000 *Nucl. Fusion* **40** 295
[11] Baker D. *et al* 2000 *Nucl. Fusion* **40** 1003
[12] Kadomtsev B.B. 1975 *Sov. J. Plasma Phys.* **1** 295
[13] Cordey J.G. *et al* 1996 *Plasma Phys. Control. Fusion* **38** A67
[14] Connor J.W. and Taylor J.B. 1977 *Nucl. Fusion* **17** 1047
[15] Suttrop W. *et al* 2000 *Plasma Phys. Control. Fusion* **42** A97
[16] Yushmanov P.N. *et al* 1990 *Nucl. Fusion* **30** 1999
[17] Saibene G. *et al* 2001 The effect of plasma shape on density and confinement in JET *28th EPS Conf. on Controlled Fusion and Plasma Physics (Madeira, Portugal)* http://www.cfn.ist.utl.pt/EPS2001/fin/pdf/OR.28.pdf
[18] Beurskens M.N.A. *et al* 2000 Edge electron temperature and density mesurements for ITER shapestudies using the JET edge LIDAR system *27th Conf. on Controlled Fusion and Plasma Physics (Budapest, Hungary, 2000)*
[19] Beurskens M.N.A. *et al* 2001 Analysis of plasma edge profiles at JET *28th Conf. on Controlled Fusion and Plasma Physics (Madeira, Portugal)* http://www.cfn.ist.utl.pt/EPS2001/fin/pdf/P3.084.pdf
[20] Porter G.D. *et al* 2001 *Phys. Plasmas* **5** 1410
[21] Neuhauser J. *et al* 1999 Analysis of high-resolution ASDEX Upgrade edge plasma profiles *26th Conf. on Controlled Fusion and Plasma Physics (Maastricht, ECA)* vol 23J
[22] JET Team (prepared by K.-D. Zastrow) 1999 *Nucl. Fusion* **39** 1891
[23] Lackner K. 1994 Comments *Plasma Phys. Control. Fusion* **15** 359
[24] Stangeby P. 2000 *The Plasma Boundary of Magnetic Fusion Devices* (Bristol and Philadelphia: Institute of Physics Publishing)
[25] Boedo J. *et al* 2001 *Phys. Plasmas* **8** 4826
[26] Krasheninnikov S. 2001 *Phys. Lett.* A **283** 368
[27] Becker G. 1996 *Nucl. Fusion* **36** 1751
[28] Becker G. 1999 *Nucl. Fusion* **39** 95
[29] Dux R. *et al* 2000 Measurement of impurity transport coefficients in the confined plasma of ASDEX Upgrade *18th International Conf. on Plasma Physics and Controlled Nuclear Fusion Research (Sorrento)* CD-ROM file EXP5/32, http://www.iaea.org/programmes/ripc/physics/fec2000/ html/node1.html
[30] Sunn Pedersen T. *et al* 2000 *Nucl. Fusion* **40** 1795
[31] Taroni A. *et al* 1999 Integrated core-edge modelling of energy confinement degradation and particle content saturation in JET ELMy H-modes *26th Conf. on Control. Fusion Plasma Phys. (Maastricht, ECA)* vol 23J
[32] Mahdavi M. *et al* 2001 High performance H-mode plasmas at densities above the Greenwald limit *Proc. 18th IAEA Fusion Energy Conf. on (Sorrento, Italy, 2000)* CD ROM file EXP1/04, http://www.iaea.org/programmes/ripc/physics/fec2000/node1.htm
[33] Groebner R.J. 2002 *Phys. Plasmas* **9** 2134–40
[34] Müller H.-W. *et al* 2001 Improved edge density profiles by the Li-beam on ASDEX Upgrade *28th EPS Conf. on Controlled Fusion and Plasma Physics (Madeira, Portugal)* http://www.cfn.ist.utl.pt/EPS2001/fin/pdf/P1.109.pdf
[35] Labombard B. *et al* 2000 *Nucl. Fusion* **40** 2041
[36] Endler M. *et al* 1995 *Nucl. Fusion* **35** 1307
[37] Neuhauser J. *et al* 2002 *Plasma Phys. Control. Fusion* **44** 855–69
[38] Kurzan B. *et al* 2000 *Plasma Phys. Control. Fusion* **42** 237
[39] Scott B. 1997 *Plasma Phys. Control. Fusion* **39** 1635
[40] Bishop C.M. 1986 *Nucl. Fusion* **26** 1063
[41] Greenwald M. *et al* 1999 *Phys. Plasmas* **6** 1943
[42] Becoulet M. *et al* 2002 *Plasma Phys. Control. Fusion* **44** A103